Measurements of High-Temperature Silane Pyrolysis Using SiH_4 IR Emission and SiH_2 Laser Absorption

Eric L. Petersen*,† and Mark W. Crofton‡

Space Materials Laboratory, The Aerospace Corporation, El Segundo, California 90245, and Mechanical, Materials & Aerospace Engineering, University of Central Florida, P. O. Box 162450, Orlando, Florida 32816

Received: February 27, 2003; In Final Form: August 14, 2003

The thermal decomposition of silane highly diluted in argon was observed behind reflected shock waves over the temperature range from 1060 to 1730 K and pressures between 0.6 and 5.0 atm, making this the first SiH_4 decomposition study to thoroughly investigate pressures above 1 atm. Silane and silylene time histories were monitored using the infrared emission of SiH_4 near 4.7 μm and laser absorption of a SiH_2 $\tilde{A}-\tilde{X}$ transition near 579 nm. Reaction rate coefficients for the first- and second-order forms of the decomposition reaction $SiH_4 + M = SiH_2 + H_2 + M$ were determined from the species measurements for M = Ar. The effects of competing reactions were considered using a detailed reaction mechanism. The bimolecular rate constant over the pressure range considered herein was determined to be $k_{1a} = 7.2 \times 10^{15} \exp(-E/RT)$, with k_{1a} in cm^3/mol s and $E = 45.1 \pm 1.2$ kcal/mol. This second-order rate coefficient describes the silane decomposition reaction over the entire range of temperatures and pressures herein and shows good agreement with the results of previous studies at similar temperatures as well as those at lower pressures and at temperatures above and below the values herein. The implication of the second-order reaction rate is that the silane decomposition is still in the low-pressure limit at total mixture pressures as high as 5 atm. A pressure-dependent rate is therefore not needed for SiH_4 decomposition over a wide range of conditions of practical interest when the reaction is simply expressed in the bimolecular form.

Introduction

Because of its importance as a source of silicon in the materials processing industry and in the manufacture of glass containing silicon oxides, the thermal decomposition of gaseous silane has received much attention in recent years. Among those investigations are the early reaction vessel experiments of Hogness et al.[1] and Purnell and Walsh,[2] several high-temperature shock-tube studies,[3−11] RRKM calculations,[11−13] and various other experimental works.[14−16] Within these and related studies, it was conjectured and proven that the initial decomposition of SiH_4 over the temperature range of interest (<2000 K) forms a silylene radical and a hydrogen molecule[2,17,18]

$$SiH_4 + M = SiH_2 + H_2 + M \qquad \text{(R1a)}$$

where M is any third-body collision partner when written as a second-order reaction. However, the rate of silane decomposition for pressures less than 1 atm is often expressed in the literature in terms of the reaction rate for the unimolecular decomposition, reaction 1b

$$SiH_4 = SiH_2 + H_2 \qquad \text{(R1b)}$$

Although most researchers express the silane decomposition as R1b with some pressure dependence, there is some discrepancy as to whether the reaction is in the pressure-dependent falloff region at pressures on the order of a few atm or below.[7,9,11−13] Care must therefore be taken when using a reaction rate for reaction 1b within a larger chemical kinetics mechanism; that is, certain rates quoted in the literature for reaction 1b are only valid for the pressure of that study. The pressure dependence can be estimated if the low- and high-pressure limits were available and utilized in the method of Troe,[19] for example, or if some other method were used as in Coltrin et al.[20] Unfortunately, most of the analytical studies of silane pyrolysis in the falloff region and high-pressure limit are based on the early shock-tube experiments of Newman et al.,[3,4] whose rate coefficient (according to other researchers) appears to be an order of magnitude larger than recent shock-tube experiments,[10] further clouding the issue.

When the conditions are such that the reaction is sufficiently close to the low-pressure limit, the reaction rate constant, k_{1a}, of the bimolecular reaction is not pressure-dependent and can be expressed in the usual Arrhenius form

$$k_i = A \exp(-E_a/RT) \qquad (1)$$

In eq 1, k_i is the rate constant of reaction i, A is the preexponential constant, E_a is the activation energy in kcal/mol, R is the universal gas constant, and T is the temperature in K. The units of eq 1 are cm^3/mol s for bimolecular reactions and s^{-1} for unimolecular reactions. An overview of previous measurements of SiH_4 decomposition, including temperature and pressure ranges and the resulting activation energies, is provided in Table 1.

For the activation energy, Purnell and Walsh[2] measured a value of 51.2 kcal/mol (for k_{1b}) over a temperature range from 648−703 K and pressures from 0.05−0.30 atm, and Meunier et al.[14] found a value of 46.0 kcal/mol from their laser-induced chemical vapor deposition experiment (723−848 K). In the first

* To whom correspondence should be addressed. E-mail: petersen@mail.ucf.edu.
† University of Central Florida.
‡ The Aerospace Corporation.

10.1021/jp0302663 CCC: $25.00
Published on Web 11/14/2003

TABLE 1: Summary of Measurements of SiH_4 Decomposition

workers	ref	E_a (kcal/mol)	temp. (K)	press. (atm)	method
Hogness et al. (1936)	1	51.7	653−763	<1.0	reaction vessel
Purnell and Walsh (1966)	2	51.2	648−703	0.05−0.3	reaction vessel
Newman et al. (1978)	3	56.1	1200−1300	5.0	shock tube
Newman et al. (1979)	4	52.7	1035−1184	5.3	shock tube
Tanaka et al. (1983)	5	39.4	1700−3900	0.1−0.5	shock tube
Votintsev et al. (1987)	6	64.5	1400−1800	1.0	shock tube
Tanaka et al. (1987)	7	48.1	1250−1600	0.25−1.3	shock tube
Meunier et al. (1987)	14	46.0	723−848	0.006−0.013	LI CVD reactor
Koshi et al. (1991)	9	38.1	1188−1574	0.18−1.2	shock tube
Mick et al. (1993)	10	48.0	1250−1715	0.7	shock tube
Han et al. (1996)	15	39.9	623−748	0.001−0.004	reaction vessel
Petersen and Crofton (2003)	this study	45.1	1060−1730	0.6−5.0	shock tube

shock-tube studies of silane decomposition, Newman et al.[3,4] obtained (for k_{1b}) a value of 56.1 kcal/mol in their earlier paper (1200−1300 K, 5.0 atm) and 52.7 kcal/mol in their later paper (1035−1184 K, 5.3 atm). At much higher temperatures and over a much wider range (1700−3900 K), Tanaka et al.[5] found the activation energy of k_{1a} to be 39.4 kcal/mol. In a later study, Tanaka et al.[7] measured a value of 48.1 kcal/mol for temperatures between 1250 and 1600 K. Similarly, Koshi et al.[9] in their shock-tube study (1190−1570 K) noted activation energies between 37.1 and 39.2 kcal/mol for k_{1b}, depending on the total mixture pressure. More recently, Mick et al.[10] used atomic resonance absorption spectroscopy of H and Si atoms to determine an activation energy of 48.0 kcal/mol for k_{1a} for reflected-shock temperatures between 1250−1715 K at a single pressure of 0.7 atm. These varied results for E_a may depend to some extent on the temperature range, the pressure range, and competing reactions.

The purpose of the present study was to perform a series of shock-tube experiments over a range of temperatures (≅1100−1700 K) and pressures (≅0.6−5.0 atm) to determine the reaction rate constant of silane pyrolysis and its pressure dependence. To conduct the study, the authors utilized a combination of established shock-tube techniques, nonintrusive optical diagnostics for species concentration measurements, and modern chemical kinetics modeling. To the authors' knowledge, the present work was the first study to use a detailed kinetics model of the secondary reactions while determining the rate of silane pyrolysis from the shock-tube data. Details of the experimental apparatus and procedure are described first, followed by an analysis of the silane decomposition kinetics and competing reactions. The results of the experiment are given in terms of species concentration profiles and curve fits of the reaction rate constant for silane decomposition, and the results are compared with previous studies. A discussion of the apparent pressure dependence is also included.

Apparatus and Procedure

A stainless steel shock tube was utilized for the experiments. The pressure-driven shock tube operated with helium as the driver gas and has a driver length of 3.5 m with an internal diameter of 7.62 cm. The 10.7-m test section has an internal diameter of 16.2 cm. Lexan diaphragms ranging from 0.1−0.5 mm thick were utilized to produce reflected-shock pressures from approximately 0.4 to 5 atm. Typical test-section fill pressures were on the order of 5−100 Torr and were monitored with one of three MKS Baratron model PDR-C-1B pressure transducers with ranges from 0−10, 0−100, and 0−1000 Torr. All measurements, described below, were performed exclusively behind reflected shock waves at a location 1.6 cm from the endwall.

Purity of the driven-section volume was maintained by a 1000-L/s Leybold TMP1000C turbomolecular pump, and ultimate pressures below 5×10^{-7} Torr were obtained via overnight pumping. Typical pre-experiment fill pressures were at least 5×10^{-6} Torr with a worst-case combined leak and outgassing rate of 2×10^{-5} Torr/min. To minimize the possibility of impurities leaking into the test gas, experiments were routinely performed within 30 s of filling the tube.

Because the products of silane decomposition are condensed silicon hydrides in the form of a light powder film, care was taken to clean the inner walls of the shock-tube driven section every 1−2 experiments. However, exploratory tests were still performed to determine what impact, if any, the residual powder on the shock-tube walls would have on subsequent experiments if a rigorous cleaning procedure were not followed. It was deduced that, because the initial silane concentrations were very small (see below), the buildup of residual powder from up to a half dozen previous experiments had a negligible impact on the results.

Temperatures behind the reflected shock wave were determined from direct measurement of the incident-shock velocity. Five fast-response (<1 μs) piezoelectric pressure transducers (PCB 113A) were used to trigger four time-interval counters (Fluke PM6666), providing four axial measurements of the shock speed. Using the velocity extrapolated to the endwall in conjunction with the standard one-dimensional shock relations and the Sandia thermodynamic database,[21] the temperature and pressure behind the reflected shock wave were determined. The uncertainty in the test temperature is on the order of 5 K for the conditions of this study.

Small amounts of research-grade SiH_4 (300−1030 ppm) highly diluted in ultrahigh purity argon were used as the test-gas mixtures. These mixtures were produced manometrically using partial pressures in a mixing tank to a total pressure of approximately 6 atm. The overall uncertainty in the volume fraction of silane was less than 1% using the Baratron vacuum pressure transducers described above.

Species Measurements

Two species were monitored during the experiments: SiH_4 and SiH_2. For the SiH_4 concentration measurements, an infrared-emission technique was used. Emission from the well-known ν_3 Si−H vibrational stretch mode was monitored by a fast-response (<1 μs), LN_2-cooled InSb detector (Judson J10D) with a 1-mm element. A filter centered at 4.7 ± 0.1 μm was used to distinguish the SiH_4 emission from background radiation. The emitted light from the shock tube gases was focused onto the detector through a CaF_2 window and a 2-mm slit to improve the time resolution of the measurement and minimize scattered radiation from the shock-tube walls. A similar IR-emission

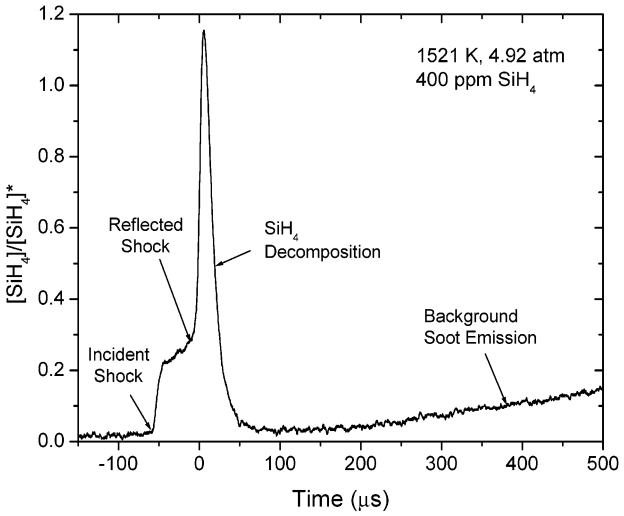

Figure 1. Infrared emission trace for SiH_4 concentration showing prominent features.

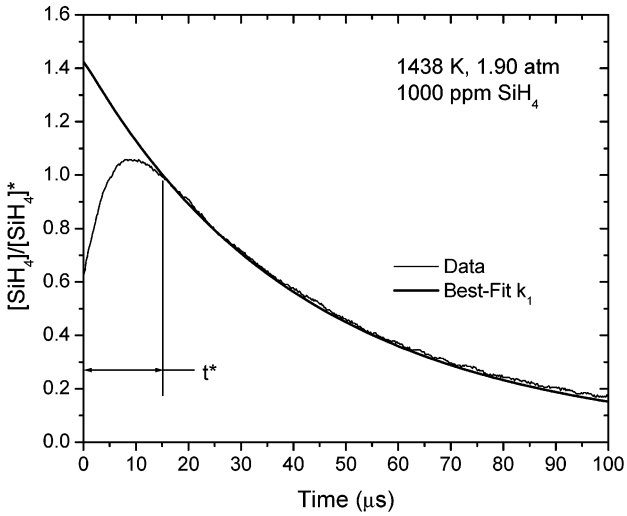

Figure 2. Typical normalized SiH_4 concentration time history and comparison with silane pyrolysis model (Table 2).

technique has been employed in other shock-tube measurements of silane decompostion.[5,7−9] These earlier studies have shown that the possibility of interference emission from other Si_xH_y molecules is negligible over similar SiH_4 concentration ranges.

Figure 1 gives a sample IR-emission measurement showing key features. Arrival of the incident and reflected shocks is evident in the emission trace. For the reflected-shock temperature shown (1521 K), the silane quickly decomposes after arrival of the reflected shock at time $t = 0$. At longer times, broadband interference emission from condensed Si_xH_y particles is evident. However, interference emission from the soot particles (which do not form until most of the silane has decomposed) was proven during the course of the experiments not to affect the kinetics measurements that utilize the emission data at earlier times.

Assurance that the soot emission did not interfere with the determination of the decomposition rate was accomplished by comparing rates obtained from the data traces in two ways: (1) from the raw emission traces and (2) from the emission traces with a correction for the soot emission. The soot correction was performed by extrapolating the long-time emission trend (Figure 1) back to time zero and subtracting it from the overall measured signal level. From such calculations, the decomposition rates obtained at the early times (typically < 100 μs) using both methods were nearly identical within the stated accuracy of the final rate herein.

Premature decomposition of the silane behind the incident shock wave, prior to arrival of the reflected shock wave, was not a problem for the temperature range of the present experiments. For example, at the maximum reflected-shock temperature and pressure of this study (1730 K, 5 atm), a 1000-ppm mixture of SiH_4 in argon would be exposed to incident-shock conditions on the order of 900 K and 1 atm. As shown in Figure 1, the typical duration of the mixture at the incident-shock conditions prior to reflected-shock arrival is about 50 μs. Kinetics calculations at these conditions and for this time duration indicate that the decomposition of SiH_4 is imperceptible ($\ll$0.1%). (In fact, it takes over 200 μs for 0.1% of the silane to decompose at the extreme conditions of this example.)

To minimize effects near time zero immediately after passage of the reflected shock wave, the emission signals were normalized to the measured light intensity at a later time t^*. This normalization procedure, defined in Figure 2 for a typical silane decomposition measurement, is based on the fact that the measured intensity (in volts) is proportional to the species mole fraction, assuming a simple harmonic oscillator model as follows:

$$I'(t) \propto \frac{1}{(e^{\theta_v/T} - 1)}\left[\frac{X_{SiH_4}(t)}{RT}\right] \tag{2}$$

In eq 2, $I'(t)$ is the instantaneous IR light intensity at time t, θ_v is the characteristic vibrational temperature of the ν_3 transition, and $X_{siH4}(t)$ is the mole fraction of silane at time t. Because eq 2 applies to any time t, and the temperature is constant to within a few Kelvins over the shock-tube experiment for the highly diluted mixtures utilized, one can normalize the $I'(t)$ to the value at some time t^*:

$$\frac{I'(t)}{I'(t^*)} \propto \frac{X_{SiH_4}(t)}{X_{SiH_4}(t^*)} = \text{constant } X_{SiH_4}(t) \tag{3}$$

In this fashion, the measured SiH_4-emission signals can be compared directly with the chemical kinetics model to infer the reaction rate coefficient, discussed in more detail below and displayed in Figure 2. Note that the time response of the emission setup is only limited near time zero, during the passage of the shock wave. The actual time response of the detector is <1 μs otherwise.

The other species measured was the key intermediate radical, SiH_2. A conventional shock-tube laser-absorption setup based on differential absorption and common-mode rejection, as in Dean and Hanson,[22] was employed in experiments separate from the SiH_4 emission measurements. A key SiH_2 transition near 579 nm has already been identified in a similar laser-absorption experiment by Markus and Roth[23] and was duplicated herein. The transition of interest was the $^rQ_{0,4}(4)$ line in the $\tilde{A}-\tilde{X}$ (0,2,0)−(0,0,0) band at 17 260.82 cm^{-1}.

Figure 3 shows the basic laser absorption setup. A Coherent 699−21 ring-dye laser operating on Rhodamine 590 dye, pumped by all lines of a Coherent Innova I-20 argon-ion laser, was the tunable light source. A sample of the beam was sent to a Burleigh WA-4500 wavemeter to monitor the wavelength with a resolution of 0.005 cm^{-1}, and the main beam was focused through the CaF_2 windows in the shock tube to a diameter on the order of 1 mm. The incident laser intensity, I_0, and the transmitted intensity, I, were monitored by Si photodiodes with

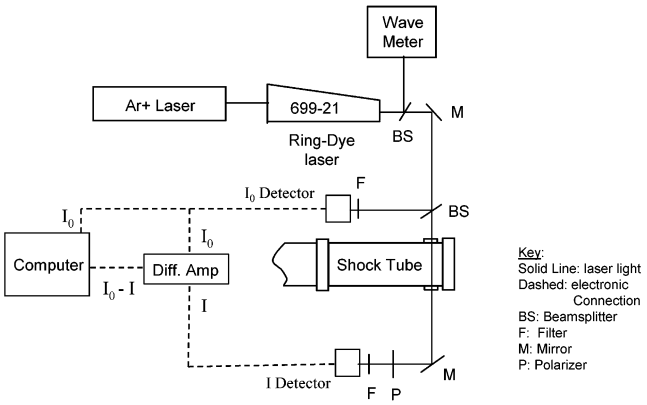

Figure 3. Laser absorption setup for the measurement of SiH_2 concentration.

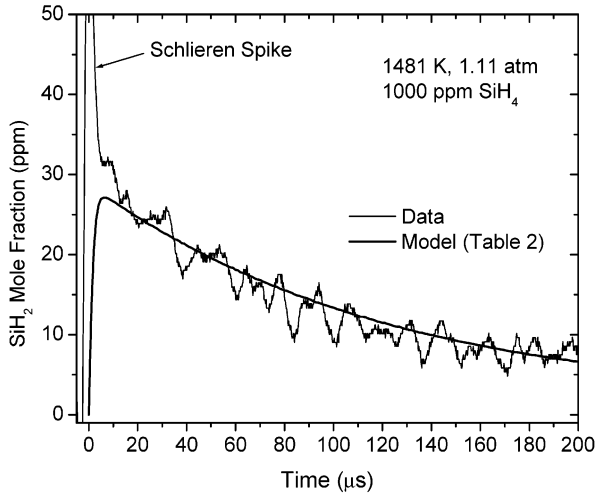

Figure 4. Typical SiH_2 mole fraction time history and comparison with the silane pyrolysis model (Table 2).

a 1-MHz bandwidth (New Focus model 2031). A differential preamplifier (SRS SR560) was used to take the differential absorption signal, $I_0 - I$, and this difference signal along with I_0 were sent to separate channels on a computer-based oscilloscope consisting of two CS512 boards from Gage Applied Sciences (4 channels total).

A typical SiH_2 absorption signal is displayed in Figure 4. In all experiments over the temperature and concentration ranges investigated herein, the SiH_2 formed immediately after passage of the reflected shock wave at $t = 0$. At time zero, passage of the requisite density gradient of the reflected shock wave through the laser beam caused temporary beam steering and, hence, some extinction of the laser light; this phenomenon is identified as the Schlieren spike in Figure 4 and lasted approximately 3−5 μs in most experiments. Signal-to-noise ratios between 5 and 10 were achieved in the absorption experiments, corresponding to a resolution of approximately 0.5−1.0% absorption or about 1−5 ppm, depending on the conditions (about ±3 ppm in Figure 4). The peak SiH_2 concentration in Figure 4 corresponds to approximately 5% absorption.

A spectroscopic model of the SiH_2 absorption, based primarily on the model given in Markus and Roth,[23] was developed to convert the absorption signals to mole fractions. Applying Beer's law to the shock-tube experiment, the differential absorption measurement is related to the absorption coefficient at frequency ν (cm^{-1}), the total pressure behind the reflected shock, P, the SiH_2 mole fraction, X_{siH2}, and the optical path length, L (16.2 cm):

TABLE 2: Reaction Mechanism Employed for Silane Pyrolysis Calculations[a]

		rate coefficient		
no.	reaction	A	E_a	ref
1a	$SiH_4 + Ar = SiH_2 + H_2 + Ar$	7.2×10^{15}	45.1	this study
2	$SiH_2 + Ar = Si + H_2 + Ar$	9.1×10^{13}	30.2	26
3	$Si_3H_8 = SiH_2 + Si_2H_6$	7.8×10^{14}	50.9	26
4	$Si_3H_8 = H_3SiSiH + SiH_4$	5.5×10^{15}	52.0	26
5	$Si_2H_6 = SiH_4 + SiH_2$	5.2×10^{10}	33.5	26
6	$H_2 + Ar = H + H + Ar$	2.2×10^{14}	95.9	26
7	$SiH_4 + SiH_2 = H_3SiSiH + H_2$	1.3×10^{13}	0.0	26
8	$SiH_2 + SiH_2 = Si_2H_2 + H_2$	6.5×10^{14}	0.0	26
9	$SiH + H_2 = SiH_2 + H$	4.8×10^{14}	23.6	26
10	$SiH + SiH_4 = Si_2H_4 + H$	1.6×10^{14}	0.0	26
11	$Si + H_2 = SiH + H$	1.5×10^{15}	31.8	26
12	$Si + SiH_4 = Si_2H_2 + H_2$	4.0×10^{14}	0.0	26
13	$Si + Si_2H_6 = Si_3H_2 + 2H_2$	4.8×10^{14}	0.0	26
14	$H_3SiSiH = H_2SiSiH_2$	7.9×10^{12}	10.5	26

[a] $k_i = A \exp(-E_a/RT)$; cm^3, mol, s Units; E_a is in kcal/mol.

$$\frac{I_0 - I}{I_0} = 1 - \exp(-k_\nu P X_{SiH_2} L) \tag{4}$$

Describing the line shape of the transition by a Voigt profile, and assuming the frequency is at line center, it can be shown that the absorption cross section at line center as a function of T and P, $\sigma^0(T,P)$, is given by

$$\frac{\sigma^0(T,P)}{\sigma^0(T_0,P_0)} = \exp\left[-F(J'')\frac{hc}{k}\left(\frac{1}{T} - \frac{1}{T_0}\right)\right]\frac{Q_{vib}(T_0)}{Q_{vib}(T)}\left(\frac{T}{T_0}\right)^{3/2}\frac{\Phi^0(T,P)}{\Phi^0(T_0,P_0)} \tag{5}$$

where T_0 and P_0 are the reference conditions defined as 1757 K and 0.3 bar, respectively, and the reference cross section is $\sigma^0(T_0,P_0) = 1.3 \times 10^{-17}$ cm^2 per Markus and Roth.[23] In eq 5, $F(J'')$ is the term energy calculated to be 108.61 cm^{-1} (ref 23), h is Planck's constant, c is the speed of light, k is Boltzmann's constant, and Q_{vib} is the vibration partition function of a harmonic oscillator with vibrational constants ω_i taken from Colvin et al.[24] ($\omega_1 = 2032$ cm^{-1}, $\omega_2 = 1004$ cm^{-1}, $\omega_3 = 2022$ cm^{-1}).

The Voigt profiles at line center, Φ^0, are defined in the usual manner as functions of the Doppler line width, $\Delta\nu_D$, the collision line width, $\Delta\nu_c$, and the Voigt function, V. The Voigt function at line center, $V(0,a)$, was taken from the procedure defined by Pierluissi and Vanderwood.[25] Finally, the absorption coefficient from eq 4 is related to the collision cross section via

$$k_\nu = \frac{\sigma^0}{RT} = 7.337 \times 10^{21}\frac{\sigma^0}{T}\ atm^{-1}\ cm^{-1} \tag{6}$$

Further details on the spectroscopic model can be found in Markus and Roth.[23]

Chemical Kinetics

When measuring the rate coefficient of the silane decomposition, reaction 1a, modern chemical kinetics modeling techniques can be employed along with the latest rate coefficients to include the effect of competing reactions. This approach was employed in the present study using the reactions and rate coefficients for silane pyrolysis summarized in Woiki et al.[26] and listed in Table 2. All chemical kinetics calculations were performed using the constant-pressure option in the shock-wave subroutine of

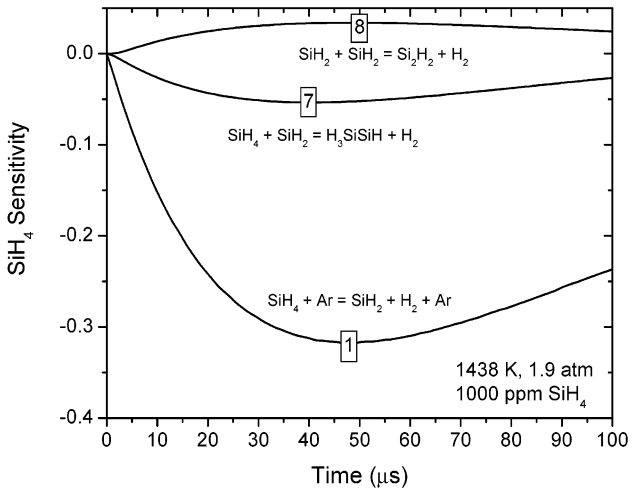

Figure 5. Sensitivity of SiH_4 concentration to the most significant reactions in the silane pyrolysis mechanism. Conditions correspond to the SiH_4 measurement in Figure 2.

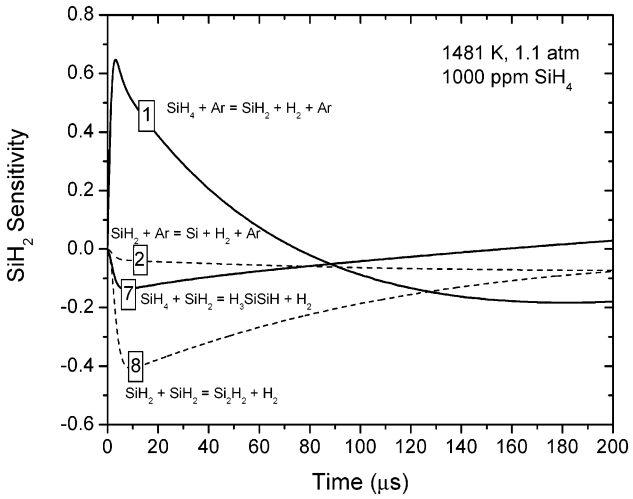

Figure 6. Sensitivity of SiH_2 concentration to the most significant reactions in the silane pyrolysis mechanism. Conditions correspond to the SiH_2 measurement in Figure 4.

the CHEMKIN software.[27] Likewise, all sensitivity analyses were performed using the SENKIN software.[27]

Although the entire mechanism in Table 2 was used in the data analysis presented herein for completeness, only a few of the 14 reactions are actually important over the temperatures and concentrations of interest. Of primary importance is the sensitivity of the measured species to reaction rate coefficients of each of the competing reactions. Figure 5 shows the sensitivity of SiH_4 to the rate coefficients of each reaction (where only the dominant reactions are shown). The conditions of the sensitivities shown in Figure 5 were calculated for the conditions corresponding to the data trace provided in Figure 2. The normalized sensitivities are defined as $(1/X_{SiH_4,max})(\partial X_{SiH_4}/\partial k_i)$, where k_i is the reaction rate coefficient of the ith reaction.

From Figure 5, the SiH_4 concentration is most sensitive to the rate of the reaction of interest, i.e.

$$SiH_4 + Ar = SiH_2 + H_2 + Ar \qquad (R1a)$$

Although the silane concentration is about six times more sensitive to R1a, the closest competing reaction is the SiH_4-removal reaction 7 involving reactions between SiH_4 and SiH_2; this reaction competes for SiH_2 radicals with the SiH_2 recombination reaction 8

$$SiH_4 + SiH_2 = H_3SiSiH + H_2 \qquad (R7)$$

$$SiH_2 + SiH_2 = Si_2H_2 + H_2 \qquad (R8)$$

The dominance of reaction R1a in the silane-concentration sensitivity supports the use of SiH_4 concentration measurements to discern the reaction rate coefficient of R1a. However, inclusion of the best-known rates for the closest competing reactions still improves the accuracy of the measurement to some extent. The additional reactions tend to accelerate the decomposition of SiH_4, so if they were ignored, the apparent rate of R1a would be mistakenly higher.

The mechanism herein assumes that the SiH_2 molecules are consumed by the decomposition reaction

$$SiH_2 + Ar = Si + H_2 + Ar \qquad (R2)$$

In recent experiments yet to be published, the authors have found that R2 is particularly important as well, although still secondary in its impact on SiH_4 time histories compared to R1a.

Similarly, a sensitivity analysis of the effect of the reactions in Table 2 on the measured SiH_2 concentrations was performed. Figure 6 presents the dominant sensitivities corresponding to the conditions of the SiH_2 data trace of Figure 4. Although k_{1a} is again the dominant reaction rate influencing the production of SiH_2 for the present conditions, reaction 8 is almost as influential as a source of SiH_2 removal. The sensitivity of SiH_2 to reaction 7 is within about 20% of the sensitivity to R1a, and the silylene decomposition (R2) reaction rate also has a sensitivity within 10%. Of course, the results of the sensitivity analysis depend on the reaction mechanism defined in Table 2.

Because the reaction rate coefficients of the competing reactions R2, R7, and R8 (Figure 6) are not well-known,[26] the use of the SiH_2 concentration measurements to discern the rate of the main silane decomposition reaction was considered secondary to the use of the SiH_4 measurements. As shown below, the SiH_2 concentration measurements were nonetheless useful in verifying the value of k_{1a} obtained herein, although the resolution of the signals was not adequate enough to simultaneously determine the rate of R8 (given the rate of R1a from the SiH_4 measurements). This issue is an ongoing one in the authors' laboratory, wherein an improved SiH_2 diagnostic based on FM absorption spectroscopy has been set up.

Results and Discussion

A total of 40 silane concentration profiles were obtained over a range of temperatures from 1063 to 1734 K and pressures from 0.6 to 5.0 atm. Eleven experiments using the SiH_2 laser-absorption diagnostic were performed for temperatures between 1240 and 1643 K and pressures from 1.2 to 2.0 atm. Using the mechanism of Table 2 and CHEMKIN, the reaction rate of R1a was altered to fit each SiH_4 profile for each test; the resulting best-fit k_{1a} was then defined as the measured k_{1a} for that test. Figure 2 shows a typical comparison between the best-fit kinetics prediction and the actual SiH_4 concentration data. The agreement shown is visibly good and representative of the entire data set.

A linear regression of the data on an Arrhenius plot is displayed in Figure 7. Each symbol in Figure 7 corresponds to a different initial SiH_4 concentration in argon. The resulting rate coefficient in the form of eq 1 is

$$k_{1a} = 7.2 \times 10^{15} \exp(-45.1/RT)\ \mathrm{cm^3/mol\ s} \qquad (7)$$

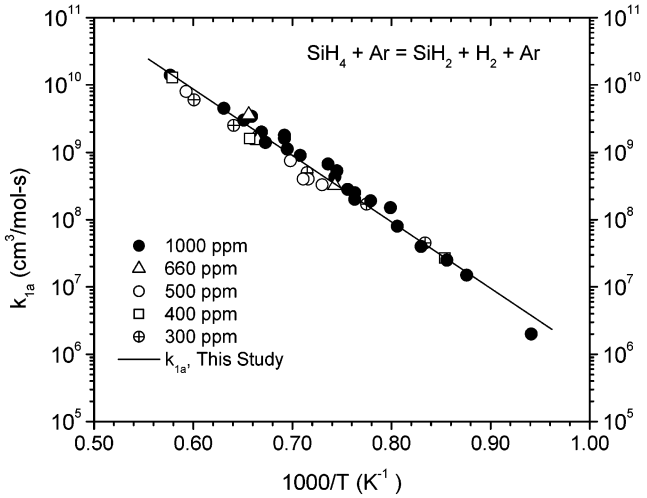

Figure 7. Arrhenius plot of the present data for the bimolecular decomposition reaction rate coefficient k_{1a}.

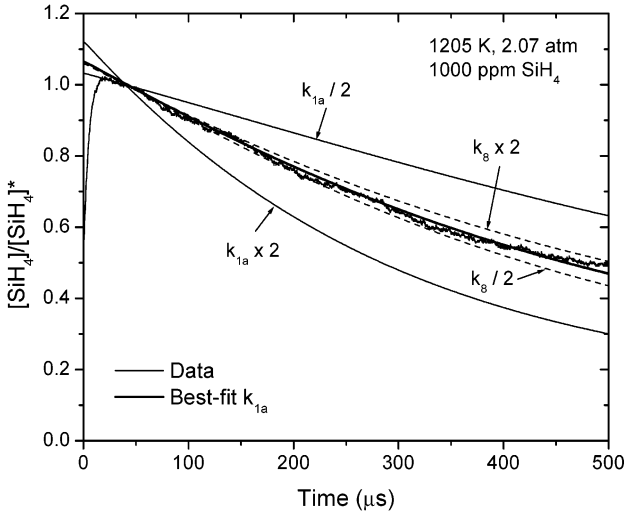

Figure 8. Effects of uncertainties in k_{1a} and k_8 on the present measurements of SiH_4 concentration.

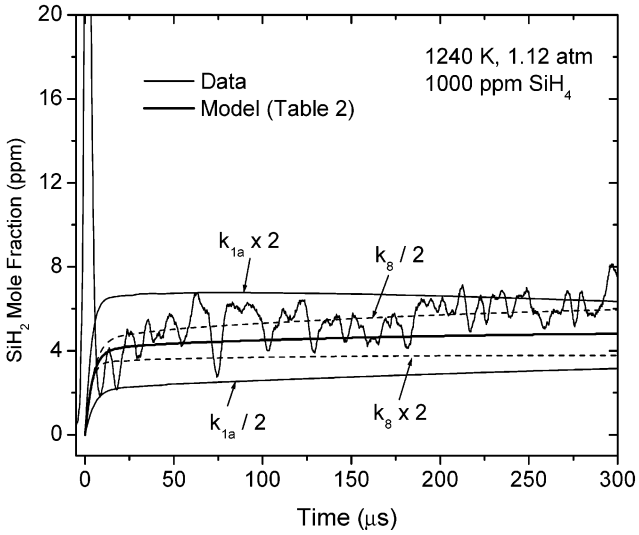

Figure 9. Effects of uncertainties in k_{1a} and k_8 on the present measurements of SiH_2 concentration.

The r^2 of this equation is 0.98, and the uncertainty in the activation energy is $\pm$1.2 kcal/mol. Referring to Figure 1, the present value of E_{a1} is near the middle of the span seen from the literature.

Equation 8 provides a rate that agrees well with those of earlier shock-tube experiments,[4,5.7,9] within about 30% or better. Conversely, the current measurement of k_{1a} is higher than but within a factor of 2 of the measurement by Mick et al.,[10] which has an activation energy of 48.0 kcal/mol. Their experiments were performed in highly diluted mixtures ($\approx$1 ppm SiH_4) and employed measurements of Si and H atoms using absorption spectroscopy. They used a reaction set including only R1 and R2 to fit their data and infer rates for each.

Possible errors and their impact on the measured k_{1a} were investigated in an attempt to justify the current E_{a1} in light of the wide range of values seen in previous studies (Table 1). For example, interference from soot emission at longer times would lead to an artificially larger SiH_4 signal at later times, resulting in a lower decomposition rate than in eq 7. Impurities in the shock-tube test section such as oxygen and/or residual particles tend to speed up the decomposition of silane. Hence, the effects of impurities would be higher for the lower-concentration SiH_4 mixtures, hence making these more-dilute mixtures show an artificially faster decomposition rate. However, this effect is also not seen in the data of Figure 7, where the 300-ppm SiH_4 mixtures produced decomposition rates similar to those of the 1000-ppm mixtures within the accuracy of the experiment.

The present silane-decomposition kinetics model agrees well with the measured SiH_2 profiles. A typical comparison is shown in Figure 4, where the agreement between the current silane decomposition rate (and Table 2 model) is well within the resolution of the SiH_2 measurement. This result is typical of most of the measured SiH_2 profiles, so further refinement of either the kinetics model or the SiH_2 spectroscopic model was not performed. The impact of differences in the measured k_{1a} by as much as a factor of 2 is shown in a representative SiH_4 profile (Figure 8) and a representative SiH_2 profile (Figure 9).

Unfortunately, the laser absorption measurements herein and in Markus and Roth[23] are not immune to the presence of particle formation, which tends to increase the level of laser extinction, making the level of SiH_2 appear artificially higher. Recent experiments by the authors using a SiH_2 diagnostic that is insensitive to particle formation show results that are somewhat different from those herein for the SiH_2 time histories. The fair agreement between the present SiH_2 results and the Table 2 model may be because some of the rates in Table 2 were obtained using the particle-tainted technique. The results of these later experiments are forthcoming in a future publication by the authors.

Although shown above to be of secondary importance, the impact of competing reactions and their lesser-known k_i can likewise be estimated. Figure 8 shows in comparison with the measured SiH_4 time history the model prediction with the rate coefficient of reaction 8 being higher and lower than the value in Table 2 by a factor of 2. The impact of such an uncertainty in k_8 is not significant. Similarly, the impact of k_8 on the prediction of a typical SiH_2 time history is shown in Figure 9. As expected, because the SiH_2 concentration is particularly sensitive to the rate of reaction 8 (Figure 6), uncertainty in its reaction rate can have a larger predicted impact on the SiH_2 profiles than on the SiH_4 profiles (although still within the uncertainty of the SiH_2 measurement).

However, as mentioned above, the authors have noticed that the value inferred for k_{1a} from the present data depends on the reaction mechanism employed. Nonetheless, even omissions of and drastic changes to the rates in Table 2 (by more than $\times$10) led to k_{1a} correlations within about 50% of the final value

extended in this paper. This robustness is testimony to the dominance of R1a seen in Figures 5 and 8.

Of particular interest is the fact that the bimolecular form of the silane decomposition reaction, R1a, can represent all of the data. This result is significant in that, for the range of total pressures up to at least 5 atm, the silane decomposition rate over the temperature range of this study (≈1000−1800 K) is in the low-pressure limit and defined by the 2nd-order reaction R1a. Therefore, over the range of most practical applications of silane combustion, the rate coefficient of the primary decomposition step is not pressure dependent. One check on this result is to correlate the data for only the lower-pressure points. When the authors excluded all data above 2 atm, the same rate coefficient expression as eq 7, within 0.2 kcal/mol and with the same preexponential factor, was obtained.

Quite often in the literature, however, silane decomposition is expressed in its unimolecular form

$$SiH_4 = SiH_2 + H_2 \qquad \text{(R1b)}$$

When written in this fashion, k_{1b} must be pressure dependent for all total pressures lower than the high-pressure limit.[19] When expressed in the form of R1b, the authors have found that the bimolecular and unimolecular rate coefficients of SiH_4 decomposition are related by the total concentration over the range of the present study, i.e, $k_{1b} = k_{1a}[M]$ (with M = Ar). This result implies that the pressure dependence of k_{1b} is linear for the present study, which agrees with the simple relationship between k_{1a} and k_{1b} derived by ignoring competing reactions

$$\frac{d[SiH_4]}{dt} = -k_{1a}[SiH_4][M] = -k_{1b}[SiH_4] \qquad (8)$$

Other investigators have also concluded that k_{1b} is linearly related to the pressure, namely Han et al.[15] and Meyerson et al.[28] As discussed in Han et al.,[15] the rate coefficient of R1b was postulated by Coltrin et al.[20] to follow the form

$$k_{1b} = (\alpha + bP)A_{1b}T^{\beta}\exp(-E_{1b}/RT) \qquad (9)$$

However, Coltrin et al.[20] found a value for α close to zero (i.e., 0.0504) and a value for *b* close to one (i.e., 0.9496) using an RRKM analysis of the experimental values of Newman et al.[3,4] for pressures from 0.006 to 1.0 atm. As a result, eq 9 predicts k_{1b} to be essentially linearly related to the pressure, as observed in the present experiments over a range of pressures from 0.6 to 5.0 atm. Tanaka et al.[7] were also able to correlate their shock-tube data by a single rate expression for k_{1a} (for pressures between 0.25 and 1.3 atm), although they observed a $P^{1/2}$ pressure dependence for k_{1b}.

An Arrhenius plot of k_{1b} obtained from the data is given in Figure 10. The data fall within four, average total-pressure groupings: 0.6, 1.0, 2.0, and 4.5 atm. The rate coefficients k_{1b} in the form of eq 1 for each pressure group are summarized in Table 3 and plotted as solid lines in Figure 10. When compared with the result for k_{1a} in eq 7, the activation energies for k_{1b} in Table 3 are about 4 kcal/mol lower and closer to 40 kcal/mol.

Another useful plot is that of k_{1b} versus pressure to discern if the reaction rate is within the falloff region between the low- and high-pressure limits from unimolecular decomposition theory. Using the curves from Table 3, the results of the present experiments are plotted versus pressure in Figure 11 for 4 different temperatures: 1100, 1300, 1500, and 1700 K. The Table 3 results (representing the measured data) are displayed as points, whereas the estimate that $k_{1b} = k_{1a}[M]$ is displayed

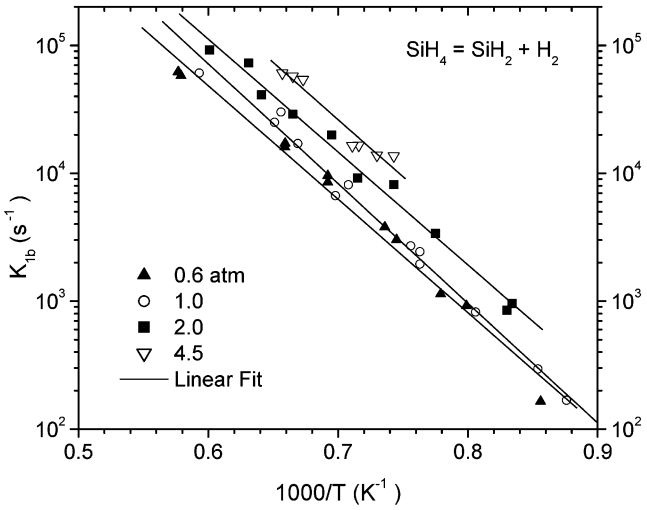

Figure 10. Arrhenius plot of the measured unimolecular decomposition rate coefficient k_{1b} at various pressures.

TABLE 3: Rate Coefficient Constants for $k_{1b} = A\exp(-E_a/RT)$ (s^{-1}) at Various Pressure Groupings[a]

P	*A*	E_a	r^2
0.6	1.1×10^{10}	40.7	0.983
1.0	3.0×10^{10}	42.8	0.991
2.0	2.2×10^{10}	40.3	0.987
4.5	5.0×10^{10}	41.0	0.943

[a] E_a is in kcal/mol, and *P* is in atm.

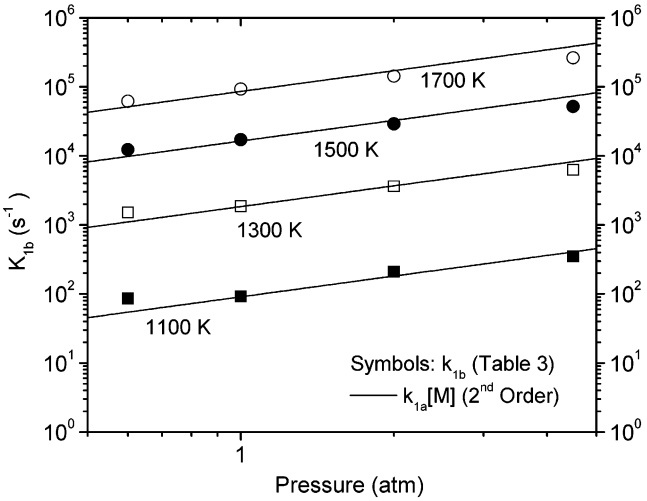

Figure 11. Unimolecular falloff plot for the k_{1b} data (Table 3) in comparison with a second-order rate coefficient, $k_{1a}[M]$.

for each temperature as lines. The good agreement between the k_{1b} results and the $k_{1a}[M]$ approximation (i.e., the bimolecular result) is further confirmation that the present results are all within the low-pressure limit of silane decomposition and not within the falloff region, even at total pressures as high as 5 atm.

Finally, the present results for k_{1a} are compared with the results of previous investigators in Figure 12. When the literature results were given in terms of k_{1b}, they were plotted in Figure 12 in terms of k_{1a} by dividing by [M] for that set of experiments. When plotted over the same temperature range, eq 7 is in good agreement with the shock-tube results of Tanaka et al.,[7] Koshi et al.,[9] and Mick et al.[10] Previous investigators have pointed out that the shock-tube data of Newman et al.[4] are an order of magnitude higher than the other, more-recent shock-tube data. However, this misconception is because their measurements

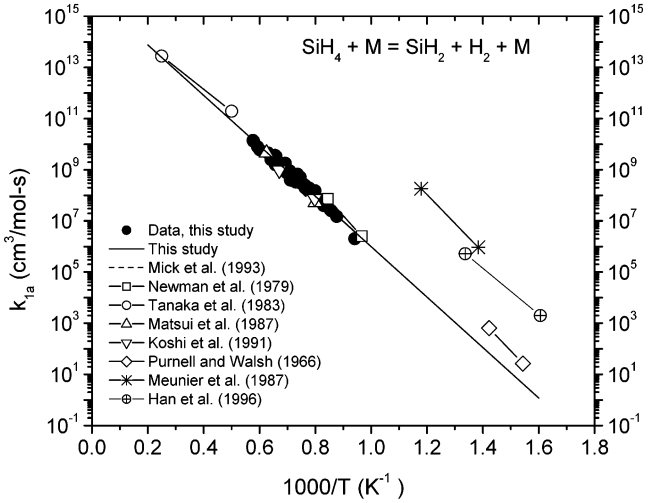

Figure 12. Comparison between the present results for k_{1a} and measurements from the literature.

were at a relatively high pressure (5.3 atm, Table 1) and were given in terms of k_{1b}. When the Newman et al. value is put in terms of k_{1a} in Figure 12 by dividing by the [M] of their study, there is good agreement with the rest of the shock-tube results.

When extrapolated to temperatures between 2000 and 4000 K, the present rate coefficient expression agrees well with the shock-tube results of Tanaka et al.[5] At lower temperatures, the present correlation agrees more with the reaction-vessel data of Purnell and Walsh[2] than with the results of Han et al.[15] and the laser-induced chemical vapor deposition experiments of Meunier et al.[14] The poor agreement of the latter studies is probably due to the indirect natures in which the rate of silane decomposition was inferred.

Summary

Silane decomposition at elevated temperatures is important in many applications such as the deposition of silicon-containing compounds, the manufacture of various glasses, and aerospace propulsion. To determine the temperature and pressure dependence of the primary silane decomposition reaction, experiments were performed behind reflected shock waves over a range of initial silane concentrations in argon between 300 and 1000 ppm, temperatures between 1060 and 1730 K, and pressures from 0.6 to 5.0 atm. Reaction progress was monitored by measuring the concentration of SiH_4 as a function of time via the emission from the ν_3 vibrational stretch mode near 4.7 μm and the concentration of SiH_2 using laser absorption of a rotational line in the $\tilde{A}-\tilde{X}$ transition at a wavelength near 579 nm. By considering the kinetics of simultaneous reactions, the rate coefficient of $SiH_4 + M = SiH_2 + H_2 + M$ (M = Ar) was determined to be $k_{1a} = 7.2 \times 10^{15} \exp(-45.1/RT)$ cm^3/mol s. This result compares favorably with established measurements in the literature, even at temperatures above and below those of the present experiments. Over the range of pressures studied, it was found that the rate of silane decomposition can be described adequately by the bimolecular form, implying that the reaction is still within the low-pressure limit at total pressures as high as 5 atm.

Acknowledgment. This work was supported by The Aerospace Corporation and The Air Force Space and Missile Systems Center under Contract No. F04701-00-C-0009. The assistance of Brian Brady in obtaining references and the invaluable help of Carrol Gardner (Aerospace) in the laboratory are recognized.

References and Notes

(1) Hogness, T. R.; Wilson, T. L.; Johnson, W. C. *J. Am. Chem. Soc.* **1936**, *58*, 108−112.
(2) Purnell, J. H.; Walsh, R., *Proc. R. Soc. London, Ser. A* **1966**, *293*, 543−561.
(3) Newman, C. G.; Ring, M. A.; O'Neal, H. E. *J. Am. Chem. Soc.* **1978**, *100*, 5945−5946.
(4) Newman, C. G.; O'Neal, H. E.; Ring, M. A.; Leska, F.; Shipley, N. *Int. J. Chem. Kinet.* **1979**, *11*, 1167−1182.
(5) Tanaka, H.; Ishigaki, A.; Asaba, T. *Shock Tubes and Waves*; Sydney Shock Tube Symposium Publishers: Sydney, 1983; pp 672−683.
(6) Votintsev, V. N.; Zaslonko, I. S.; Mikheev, V. S.; Smirnov, V. N. *Kinet. Catal.* **1987**, *27*, 843−846.
(7) Tanaka, H.; Koshi, M.; Matsui, H. *Bull. Chem. Soc. Jpn.* **1987**, *60*, 3519−3523.
(8) Koshi, M.; Yamauchi, M.; Koseki, K.; Matsui, H. *Shock Tubes and Waves*; VCH: Weinheim, Germany, 1988; pp 443−449.
(9) Koshi, M.; Kato, S.; Matsui, H. *J. Phys. Chem.* **1991**, *95*, 1223−1227.
(10) Mick, H. J.; Smirnov, V. N.; Roth, P. *Ber. Bunsen-Ges. Phys. Chem.* **1993**, *97*, 793−798.
(11) Mick, H.-J.; Roth, P.; Smirnov, V. N.; Zaslonko, I. S. *Kinet. Catal.* **1994**, *35*, 439−451.
(12) Roenigk, K. F.; Jensen, K. F.; Carr, R. W. *J. Phys. Chem.* **1987**, *91*, 5732−5739.
(13) Moffat, H. K.; Jensen, K. F.; Carr, R. W. *J. Phys. Chem.* **1991**, *95*, 145−154.
(14) Meunier, M.; Flint, J. H.; Haggerty, J. S.; Adler, D. *J. Appl. Phys.* **1987**, *62*, 2812−2821.
(15) Han, J. H.; Rhee, S.-W.; Moon, S. H. *J. Electrochem. Soc.* **1996**, *143*, 1996−2002.
(16) Onischuk, A. A.; Strunin, V. P.; Ushakova, M. A.; Panfilov, V. N. *Int. J. Chem. Kinet.* **1998**, *30*, 99−110.
(17) Neudorff, P.; Jodhan, A.; Strausz, O. P. *J. Phys. Chem.* **1980**, *84*, 338−339.
(18) Purnell, J. H.; Walsh, R. *Chem. Phys. Lett.* **1984**, *110*, 330−334.
(19) Troe, J. *J. Phys. Chem.* **1979**, *83*, 114−126.
(20) Coltrin, M. E.; Kee, R. J.; Miller, J. A. *J. Electrochem. Soc.* **1986**, *133*, 1206−1213.
(21) Kee, R. J.; Rupley, F. M.; Miller, J. A. SAND87-8215B, Sandia National Lab.: Albuquerque, NM, 1990.
(22) Dean, A. J.; Hanson, R. K. *J. Quantum Spectrosc. Radiat. Transfer* **1989**, *42*, 375−384.
(23) Markus, M. W.; Roth, P. *J. Quantum Spectrosc. Radiat. Transfer* **1994**, *52*, 783−789.
(24) Colvin, M. E.; Grev, R. S.; Schaefer, H. F.; Bicerano, J. *Chem. Phys. Lett.* **1983**, *99*, 399−405.
(25) Pierluissi, J. H.; Vanderwood, P. C. *J. Quantum Spectrosc. Radiat. Transfer* **1977**, *18*, 555−558.
(26) Woiki, D.; Catoire, L.; Roth, P. *Ceram. Process.* **1997**, *43*, 2670−2678.
(27) Kee, R. J.; Rupley, F. M.; Miller, J. A.; Coltrin, M. E.; Grcar, J. F.; Meeks, E.; Moffat, H. K.; Lutz, A. E.; Dixon-Lewis, G.; Smooke, M. D.; Warnatz, J.; Evans, G. H.; Larson, R. S.; Mitchell, R. E.; Petzold, L. R.; Reynolds, W. C.; Caracotsios, M.; Stewart, W. E.; Glarborg, P.; Wang, C.; Adigun, O. *Chemkin Collection*, release 3.6; Reaction Design, Inc.: San Diego, CA, 2000.
(28) Meyerson, B. S.; Ganio, E.; Smith, D. A.; Nguyen, T. N. *J. Electrochem. Soc.* **1986**, *133*, 1232.